Solvent-free synthesis of ZIFs compatible with iron: a route towards the elusive Fe(II) analogue of ZIF-8

Javier López-Cabrelles,[a]‡ Jorge Romero,[a]‡ Gonzalo Abellán,[a,b] Mónica Giménez-Marqués,[a] Miguel Palomino,[c] Susana Valencia,[c] Fernando Rey,[c] Guillermo Mínguez Espallargas[a]*

[a] Instituto de Ciencia Molecular (ICMol), Universidad de Valencia, c/ Catedrático José Beltrán, 2, 46980 Paterna, Spain.

[b] Department of Chemistry and Pharmacy & Joint Institute of Advanced Materials and Processes (ZMP), Friedrich-Alexander-Universität Erlangen-Nürnberg (FAU), Henkestr. 42, 91054 Erlangen and Dr.-Mack Str. 81, 90762 Fürth, Germany.

[c] Instituto de Tecnología Química (UPV-CSIC), Universitat Politècnica de València − Consejo Superior de Investigaciones Científicas, Av. de los Naranjos s/n, 46022, Valencia, Spain.

Herein we report the synthesis of an elusive metal-organic framework, the iron(II) analogue of ZIF-8, with formula Fe(2-methylimidazolate)$_2$, here denoted as MUV-3. The preparation of this highly interesting porous material, inaccessible by common synthetic procedures, occurs in a solvent-free reaction upon addition of an easily detachable template molecule, yielding single crystals of MUV-3. This methodology is extensive to other metals and imidazolate derivatives, allowing the preparation of ZIF-8, ZIF-67 and other unprecedented iron(II) ZIFs, Fe(2-ethylimidazolate)$_2$ and Fe(2-methylbenzimidazolate)$_2$. The different performance of MUV-3 towards NO sorption, compared to ZIF-8, results from the chemisorption of NO molecules, which also causes a gate opening behavior. Finally, the controlled pyrolysis of MUV-3 results in a N-doped graphitic nanocomposite that exhibits extraordinary performances for Oxygen Evolution Reaction (OER), with low overpotential at different current densities (316 mV at 10 mA·cm^{-2}), low Tafel slope (37 mV per decade), high maximum current density (710 mA·cm^{-2} at 2.0 V vs RHE) and large durability (15 h).

INTRODUCTION

The development of metal-organic frameworks (MOFs) has grown very rapidly in the last years, with numerous applications in a wide range of different fields resulting from the ample chemical versatility of this type of crystalline porous materials.[1] An interesting feature of these solids is the possibility of modifying the metal content whilst retaining the same structure, thus offering a unique opportunity to tune their physical properties. This is exemplified by the extensive family M-MOF-74, with formula M_2(dobdc) (dobdc^{4-} = 2,5-dioxidobenzene-1,4-dicarboxylate), which can be prepared for an ample range of metals, such as Mg, Mn, Fe, Co, Ni, Cu, and Zn, or combination of these.[2] Indeed, whereas Mg-MOF-74 is optimum for CO_2 capture,[3] Fe-MOF-74 is suitable for alkane/alkene separation.[4]

Zeolitic imidazolate frameworks (ZIFs) are a subfamily of MOFs consisting of tetrahedral metal centers connected by imidazolate organic ligands.[5] The most prominent member of this family is arguably Zn(Meim)$_2$ (MeimH = 2-methylimidazole),[6] also known as ZIF-8, which has a sodalite

(SOD) topology. This microporous crystalline solid has been widely studied in applications involving gas storage and separation because of its high porosity, high chemical stability, low synthetic cost and easy preparation, and is even commercially available. Four isostructural metal analogues to ZIF-8 have been reported to date: $Co(Meim)_2$ (also known as ZIF-67),[7] $Cd(Meim)_2$ (also known as CdIF-1),[8] $Mg(Meim)_2$,[9] and, more recently, $Mn(Meim)_2$.[10] However, the highly interesting iron analogue, *i.e.* $Fe(Meim)_2$, formed exclusively by iron(II) centres, has been elusive despite the vast number of potential applications of this solid, including catalysis, environmental and biomedical applications related with the low toxicity of endogenous iron(II).[11] In addition, Fe-based MOFs are good candidates for biomimetic studies with small molecules like nitric oxide and its redox transformations.[12] Indeed, all attempts to adapt the different synthetic solvent-based procedures of ZIF-8 or ZIF-67 result unfruitful when using Fe(II) instead.[13]

Considering energy-related applications, MOFs have been demonstrated as suitable precursors for fabricating heteroatom-doped nanocarbons materials (NCs) that exhibit excellent activities for catalytic reactions.[14] In particular, ZIF-derived nanocomposites have shown exceptional electrochemical catalytic activity,[15] which can be further improved with the inclusion of extrinsic iron sources before carbonization, either by insertion of iron-based molecular complexes within the pores of a ZIF, or by directly mixing the ZIF with an iron-based material.[16] Therefore, the highly porous $Fe(Meim)_2$, with a regular distribution of iron centers at atomic level, is expected to be a superior single precursor for the formation of electrocatalytic NCs.

RESULTS AND DISCUSSION

Synthesis of MUV-3. In the present work, we report for the very first time a solvent-free synthesis compatible with Fe(II) to obtain **MUV-3** (MUV: Materials of University of Valencia), the iron analogue of ZIF-8, adapting a previously described method for the preparation of non-porous iron azolates.[17] The reaction of ferrocene and 2-methylimidazole at 150 °C under vacuum, in the presence of 4,4-bipyridine (acting as a template), results after 48 h in the formation of yellow single-crystals of **MUV-3** in a quantitative manner (Figure 1a). Structural, magnetic and spectroscopic characterization unambiguously reveals the formation of the desired material. The good quality of the crystals permitted crystal structure determination by single-crystal X-ray diffraction despite the fact that the synthesis is carried out in the absence of solvents (Figure 1).

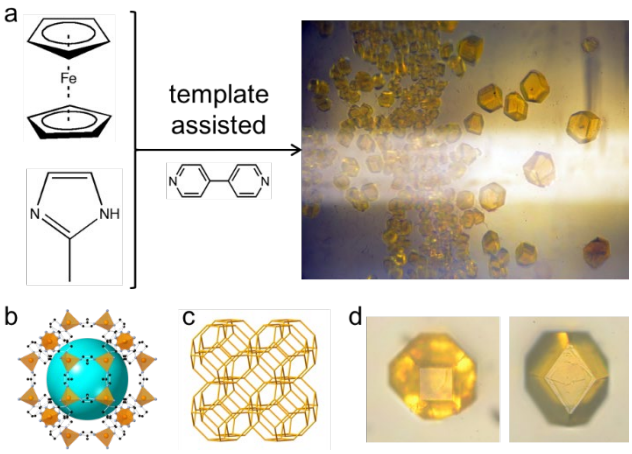

Figure 1. a) Synthetic route to form **MUV-3**. b) Crystal structure of **MUV-3**. Key: Fe, orange tetrahedra; C, black balls; N, blue balls; the blue sphere (diameter of 11 Å) represents the empty space of the structure; hydrogen atoms have been omitted for clarity. c) Sodalite topology of

MUV-3. d) Two single crystals of **MUV-3** showing the characteristic truncated rhombic dodecahedron morphology of ZIF-8 emphasizing the (100) and (110) faces.

Single-crystal X-ray diffraction analysis of the as-synthesised material reveals that the yellow crystals are isostructural to ZIF-8 (a = 17.1656(2) Å; space group $I\bar{4}3m$). Structure solution shows that each iron atom is connected to four nitrogen atoms from four imidazolate ligands (Fe–N distance of 2.032(1) Å and Fe···Fe distances of 6.069(1) Å), with voids of 2580 $Å^3$ in size, which are accessible through windows of 3.3 Å, similar to ZIF-8. Magnetic measurements indicate the presence of strong antiferromagnetic metal-metal interactions between the Fe(II) centres occurring through the imidazolate bridges (see Section S1.6). The pores of the as-synthetized single crystals contain residual electron density in the voids (estimated to be 494 electrons), which can be attributed to starting material, template and/or cyclopentadiene resulting from the reaction.

In fact, the as-synthetized bulk material presents different peak intensities in the experimental X-ray powder diffraction (XRPD) pattern as compared with the theoretical one (Figure S2), and also thermogavimetric analysis (TGA) reveals a 4 % weight loss at 200 ºC (Figure S7). A thorough activation process was therefore performed, which consisted in washing several times with dry acetonitrile for 48 h and subsequent overnight heating at 150 ºC under vacuum. This yields an activated form of **MUV-3**, as demonstrated by XRPD (Figure S2).

In contrast to ZIF-8, ZIF-67 and CdIF-1, **MUV-3** is quite sensitive to humidity in air (Figure S3), as has also been observed in Mg-ZIF-8[8] and Mn-ZIF-8.[9] Nevertheless, time-resolved XRPD study indicates that **MUV-3** is stable for a few hours in air before it starts to decompose. The stability in dry air drastically improves, pointing out humidity as the main stability issue (Figure S4). Despite this moisture-sensitivity, the compound is stable for months in inert (N_2 or Ar) atmospheres.

Remarkably, the use of 4,4'-bipyridine as template is essential for the exclusive formation of **MUV-3**; in its absence, the dense coordination polymer $Fe(Meim)_2 \cdot 0.13(FeCp_2)$ is instead obtained (Figure S5).[17d] The importance of a template in other type of solvent-free reaction (specifically mechanochemical reactions) was established by Friščić and co-workers, who showed that the presence of NH_4^+ affects the thermodynamic/kinetic product in Zn-based ZIFs.[18] We hypothesize that the presence of 4,4'-bipyridine blocks some of the coordination positions of the iron centres, thus affecting the kinetics of the crystal growth. We have screened an extensive number of templates, primarily based on pyridines, in order to examine the importance of pK_{HA}, the physical state of the template in the reaction conditions, the steric hindrance of the template and its coordination ability, establishing the importance of the latter two (see Section S1.3 in the Supporting Information). In fact, the structure-directing role of a pyridine derivative was previously observed for the formation, in solution, of ZIF-7. This MOF required the presence of 2,2´-bipyridine in order to obtain single crystals,[19] although an alternative synthetic protocol was later described without the need of such template.[5] The role of the template in modifying the kinetics of the crystal growth is consistent with SEM images, which show the formation of truncated rhombohedral crystals with well-defined shapes with variable sizes that can be controlled with the reaction time (Figure S9). Indeed, the observed crystal shapes are significantly distorted as compared with the characteristic ZIF-8 structure.[20] Such a distortion could be an effect of the template on the growth mechanism, which is currently being investigated.

Generalization of the solvent-free synthesis. The solvent-free approach here described can be expanded to the preparation of other isostructural metal analogues to **MUV-3**. Thus, using other metal sources compatible with chemical vapour deposition (CVD) techniques such as $Zn(TMHD)_2$ [TMHD = bis(2,2,6,6-tetramethyl-3,5-heptanedionato), ZnO and cobaltocene we could also obtain ZIF-8 and ZIF-67 (see Section S2.1). However, contrary to the preparation of **MUV-3**, no template is required for the formation of ZIF-8 or ZIF-67, which opens the door to reach a variety of mixed-metal structures (see Section S2).

Furthermore, the use of different imidazolate ligands allow the preparation of other unprecedented iron(II)-ZIFs with different topologies, such as $Fe(Etim)_2$ (EtimH = 2-ethylimidazole), with *qtz* topology (denoted MUV-6), and $Fe(Mebim)_2$ (Mebim = 2-methylbenzylimidazole), with *dia* topology (denoted MUV-7). This highlights the relevance of the methodology here described (see Section S2).

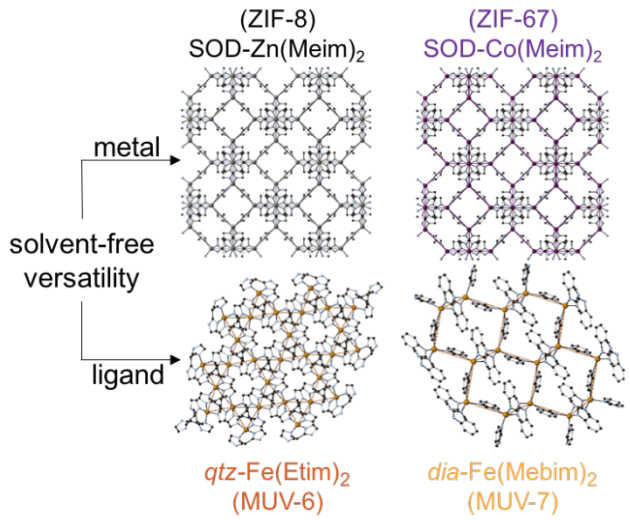

Figure 2. Expansion of the solvent-free methodology to prepare isostructural metal analogues to **MUV-3**, ZIF-8 (shown in black) and ZIF-67 (shown in purple), represented with the with *sod* topology, and different topologies of other iron(II)-ZIFs obtained with the same solvent-free methodology (MUV-6 and MUV-7, shown in dark orange and light orange respectively).

Gas sorption in MUV-3. The porous nature of **MUV-3** was assessed by N_2 sorption at 77 K. Activation of **MUV-3** prior to measurement was achieved by treating the washed material at 150 ºC under vacuum overnight. Figure 3a displays a characteristic two-step N_2 adsorption isotherm, with a plateau at 260 $cm^3 \cdot g^{-1}$, which is reminiscent to that of the analogous ZIF-8 and ZIF-67 materials. Such a similar structural response upon sorption is attributed to the flexibility of the ligands.[21] The obtained accessible surface area was calculated using the Brunauer–Emmett–Teller (BET) model, obtaining a value of 960 $m^2 \cdot g^{-1}$, which is significantly lower to that of ZIF-8 (*ca*. 1400 $m^2 \cdot g^{-1}$) likely due to the presence of organic molecules remaining in the pores. The CO_2 sorption at 298 K, shown in Figure 3b, reveals a total uptake of 2.9 $mmol \cdot g^{-1}$ at 18 bar, whereas an isosteric heat of adsorption, q_{st}, is found to be 20 $kJ \cdot mol^{-1}$ (Figure S16).

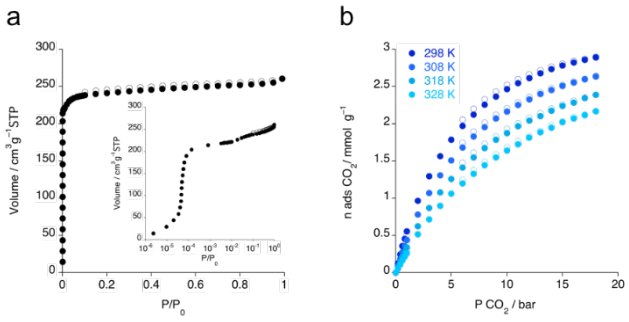

Figure 3. a) N_2 sorption (solid circle) and desorption (open circle) of **MUV-3** at 77 K. Inset: semilog plot revealing the two-step adsorption resulting from the flexibility of **MUV-3**. b) CO_2 sorption (solid circle) and desorption (open circle) isotherms at different temperatures.

Furthermore, we examined the sorption capacity of **MUV-3** towards the biologically active NO gas. **MUV-3** material was subjected to NO volumetric adsorption at 273 K, presenting a total uptake of 2.1 mmol·g^{-1} at 1 bar (Figure 4a), which corresponds to *ca*. 0.45 NO molecules per Fe^{2+} site. This suggests an incomplete NO loading, which is in agreement with the absence of a saturated plateau at 1 bar. This sorption value is lower than the exceptional storage capacity of the M-MOF-74 materials (up to 7 mmol·g^{-1}),[12,22] and similar to that of HKUST-1 (3 mmol·g^{-1}),[23] both of them presenting a high density of open metal sites. However, in sharp contrast to M-MOF-74, which shows a similar NO sorption regardless of the metal centre,[12,22] **MUV-3** has a significantly different behavior to its isostructural Zn analogue (i.e. ZIF-8). As shown in Figure 4a, the behavior of both **MUV-3** and ZIF-8 is analogous at low pressures (< 0.15 bar), with a slow progressive loading of NO, which can be attributed to physisorption. Upon further pressure increase, the amount of NO adsorbed by **MUV-3** rises sharply between 0.15 and 0.23 bar, which is not observed for ZIF-8. This is attributed to a "gate opening" effect caused by the chemisorption of NO molecules to the Fe(II) centers, unprecedented in MOFs, which typically show a constant NO sorption, even when using flexible MOFs such as MIL-88 and MIL-53.[12a,24] The NO chemisorption is evidenced by IR spectroscopy, which reveals the appearance of characteristic vibration of coordinated NO species[12] (ν_{N-O} 1720 and 1790 cm^{-1}, see Figure 4b) after exposing **MUV-3** to NO, which are absent in ZIF-8 (Figure S20). In addition, upon vacuum treatment of the NO loaded **MUV-3** and re-exposure to NO, we observe only a small sorption that can be attributed exclusively to physisorption (Figure S18), indicating that the coordinated NO molecules are retained in the structure. Interestingly, at low pressures (< 0.2 bar) the amount of adsorbed NO is larger than that observed in the first sorption cycle, indicating that the **NO-MUV-3** (i.e. **MUV-3** with chemisorbed NO) remains in the open form.

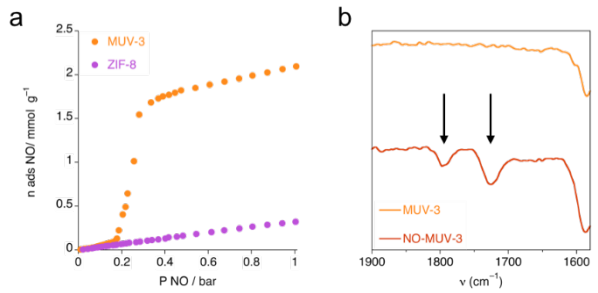

Figure 4. a) NO sorption of **MUV-3** (orange) and ZIF-8 (violet) at 273 K. b) Infrarred spectra of **MUV-3** before (light orange) and after (dark orange) exposure to NO at room temperature and ambient pressure (the analogous spectra for ZIF-8 is shown in Figure S21). The arrows indicate the appearance of characteristic vibration of coordinated NO species.

Synthesis of NC-MUV-3. Despite their typical low conductivity and relatively poor stability, which limit their use in energy storage devices, MOFs have been demonstrated as suitable precursors for fabricating heteroatom-doped nanocarbons materials that exhibit excellent electrocatalytic activities for energy-related applications.[25] In fact, ZIFs have been successfully used as templates and precursors to create N-doped nanocarbons due to their highly ordered nanoporous structure and the use of nitrogen-rich organic ligands,[26] resulting in an abundance of nitrogen incorporation which significantly enhances the electrocatalyitic performance towards oxygen reduction (ORR) and oxygen evolution (OER) reactions. In addition, as the catalyitic activity of the nanocomposites resultant from the pyrolysis of a given ZIF can be increased by iron loading in the ZIFs,[16] we investigated the electrocatalytic activity of the nanocomposite resultant from the controlled thermal treatment of **MUV-3**. In this sense, the Co analogue of **MUV-3**, ZIF-67, has been proved as an excellent precursor of N-doped carbon nanotubes with outstanding ORR and OER performance,[27] as well as bimetallic Co_xZn_{100-x}–ZIF-8,[28] or core-shell ZIF-67@ZIF-8 and ZIF-8@ZIF-67.[29,30]

The low temperature processing of **MUV-3** in a CVD oven (700 ºC for 3.5 h under N_2 atmosphere) yields a black powdered carbon material, which is subsequently treated in 0.5 M H_2SO_4 solution for 6 h in order to remove residual metals, thoroughly washed with ethanol and dried at 80 ºC (see details in Section S4). This nanocomposite (NC), denoted as **NC-MUV-3**, is exhaustively characterized (see Section S5). The formation of these nanostructures is related to the *in-situ* formation of catalytically active metallic Fe nanoparticles (NPs), detected by XRPD (Figure S23), which are originated from the presence of iron in the structure of the precursors.[31] In fact, residual Fe NPs (0.78 % according to ICP-OES analysis, Table S7) of *ca*. 10–30 nm in size that remained intact after acid leaching can be observed embedded in the carbon matrix, as shown in Figure 5a-b, and as previously observed for Co.[18] PXRD and XPS analyses of **NC-MUV-3** confirm the formation of N-doped graphitic carbon (Figure 5c). Field-emission scanning electron microscopy (FESEM) analysis shows that the previously observed defined morphology is completely lost after the thermal treatment, originating a meso/micro-porous crumpled material (Figure S25). High-resolution transmission electron microscopy (HRTEM) studies support the formation of graphitic carbon. In fact, the morphology of the sample consists of a carbon matrix composed of several graphene layers endowed with a marked corrugation, as can be observed in Figure 5. In addition, statistical Raman spectroscopy (> 7000 single point spectra) shows average values of I_D/I_G ratios of ca. 0.85, suggesting a low density of disorder and carbon defects (Figure 5d).

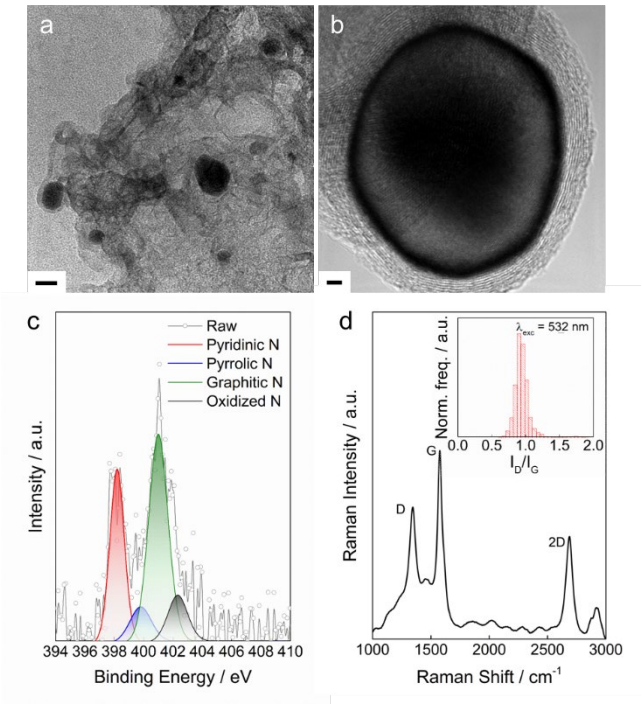

Figure 5. a) HRTEM of **NC-MUV-3** (general overview), showing the presence of the carbon matrix with embedded encapsulated Fe NPs; the scale bar is 20 nm. b) High magnification HRTEM of one Fe NP of *ca*. 30 nm surrounded by a carbon shell consisting of *ca*. 10 graphene layers; the scale bar is 2 nm. c) XPS high-resolution N1s spectrum. d) Averaged Raman spectra of **NC-MUV-3** (~7600 single-point spectra). Inset shows the corresponding I_D/I_G ratio distribution histogram (λ_{exc} = 532 nm).

Oxygen evolution reaction of NC-MUV-3. The electrocatalytic performance of **NC-MUV-3** towards oxygen evolution reaction (OER) was repeatedly tested in two different basic mediums (1 and 0.1 M KOH) in a standard three-electrode cell. For comparative purposes, we prepared working electrodes consisting of **NC-MUV-3** and other materials, including other ZIF-derived electrocatalysts and commercial catalysts. **NC-MUV-3** was investigated by linear sweep voltammetry (LSV) showing an excellent electrochemical performance. The polarization curves, depicted in Figure 6a, show low onset potentials of 1.588 and 1.541 V vs. reversible hydrogen electrode (RHE) for the 1 and 0.1 M KOH, respectively (see also Figure S34). An overpotential of 316 mV (1.542 V vs RHE) and 335 mV (1.561 V vs RHE) are required at j = 10 mA·cm^{-2} for **NC-MUV-3** in 1 and 0.1 M KOH, respectively. These values are much lower than other of ZIF-derived electrocatalysts (see Tables S9 and S10 for a complete list of MOF-derived nanocomposites and other relevant materials). A current density of 331 mA·cm^{-2} at 0.74 V (2.0 V vs RHE) is obtained in 0.1 M KOH, a value over 500 % better than the analogous NC-ZIF-67 (Figure 6a),[32] also surpassing the values obtained for the benchmark electrocatalyst in basic medium, NiFe-based oxyhydroxides (NiFeOOH; see Figure S34).[33] In addition, a maximum current density of 710 mA·cm^{-2} is found in 1 M KOH, a great value taking into account the large values of current density required for the development of oxygen evolution electrodes (>500 mA·cm^{-2}),[34] which is of the order of magnitude of NiFeOOH. The excellent catalytic activity of **NC-MUV-3** is also reflected in the Tafel slopes (Figure 6b), showing values in the range of 37 and 48 mV per decade in 1 and 0.1 M KOH, respectively, extremely low values much smaller than NiFeOOH (71 and 91 mV per decade in 1 and 0.1 M KOH, respectively) and related MOF-derived nanocarbon-based electrocatalysts, indicative of superior kinetics for the OER (see Tables S9 and S10). Finally,

Figure 6c shows a high stability and durability of **NC-MUV-3** at constant current densities *j* of 10 and 15 mA·cm^{-2} and with a constant overpotential, η, of 300 and 400 mV for 15 hours (see Figure S37 for further information). The remarkable electrochemical OER performance is mainly attributed to the synergistic effect from chemical composition and the robust porous structure composed of micro- and mesopores as well as crystalline nitrogen-doped few-layers graphene.

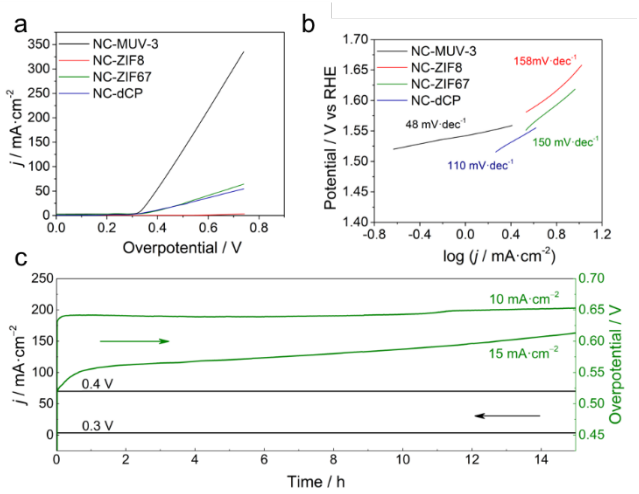

Figure 6. a) Polarization curves of **NC-MUV-3**, NC-ZIF-8, NC-ZIF-67 and NC-dense-CP measured in 0.1 M KOH; values for different conditions of pyrolysis, and comparison with benchmark catalysts can be found in the Supporting Information (section S6). b) Tafel plots highlighting the corresponding values of Tafel slopes. c) Potentiostatic (in green) and galvanostatic (in black) stability tests under a certain potential or current density of **NC-MUV-3** in 0.1 M KOH.

CONCLUSIONS

In summary, we have presented the solvent-free synthesis of the highly interesting iron(II) analogue of ZIF-8, **MUV-3**, inaccessible through conventional preparation routes, thus paving the way for its exploration in many applications. The presence of a template is crucial for the facile synthesis of phase pure single crystals of **MUV-3**, which show a gate opening behaviour analogous to that of ZIF-8. However, its behaviour towards NO sorption is completely different due to the presence of Fe(II) centres, revealing a chemisorption of the NO molecules to the metal centres. The synthetic procedure here presented, using ferrocene as the source of iron, is also compatible with the chemical vapour deposition (CVD) techniques commonly used in microelectronics and recently shown to be effective with MOFs,[35] thus facilitating its applicability. Finally, upon controlled pyrolysis at 700 °C, the synergistic effect of the highly ordered nanoporous structure, the use of nitrogen-rich organic ligands and the presence of Fe(II), causes the formation of a nanocomposite that shows an extraordinary performance in electrocatalytic water splitting. The low-cost materials used here, together with the low-temperature methodology and the facile processing, opens the possibility of using this novel material as a cheap alternative to current electrocatalysts.

EXPERIMENTAL SECTION

All reagents were commercially available and used without further purification.

Synthesis of MUV-3. Ferrocene (30 mg, 0.16 mmol), 4,4-bipyridine (50 mg, 0.32 mmol, or an alternative template, see Section S1.3 in the Supporting Information) and 2-methylimidazole (25

mg, 0.30 mmol) were combined and sealed under vacuum in a layering tube (4 mm diameter). The mixture was heated at 150 °C for 4 days to obtain yellow crystals suitable for X-ray single-crystal diffraction. The product was allowed to cool to room temperature, and the layering tube was then opened. The unreacted precursors were extracted with acetonitrile and benzene, and **MUV-3** was isolated as yellow crystals (yield 20 %). Phase purity was established by X-ray powder diffraction. Details on the thermogravimetric, SEM and magnetic analyses can be found in the Supporting Information.

ZIF-8, ZIF-67, **MUV-6** and **MUV-7** were synthesised in an analogous manner adapting the previous procedure (see section S2 in the Supporting Information).

Single Crystal diffraction. Single crystals of **MUV-3, MUV-6** and **MUV-7** were mounted on cryoloops using a viscous hydrocarbon oil to coat the crystals. X-ray data were collected at 120 K on a Supernova diffractometer equipped with a graphite-monochromated Enhance (Mo) X-ray Source (λ = 0.71073 Å). The program CrysAlisPro, Oxford Diffraction Ltd., was used for unit cell determinations and data reduction. Empirical absorption correction was performed using spherical harmonics, implemented in the SCALE3 ABSPACK scaling algorithm. Crystal structures were solved and refined against all F^2 values by using the SHELXTL and Olex2 suite of programs.[36] Non-hydrogen atoms were refined anisotropically and hydrogen atoms were placed at calculated positions (riding model). Solvent mask protocol in Olex 2 was implemented to account with the remaining electrondensity corresponding to disordered molecules of starting material in **MUV-3**. A total of 494 electrons were found un-accounted in the model (in a cavity of 2580 $Å^3$ in size). A summary of the data collection and structure refinements is provided in Tables S1 and S3. CCDC-1825894 (**MUV-3**), -1899778 (**MUV-6**) and -1899779 (**MUV-7**) contain the supplementary crystallographic data for this paper. These data can be obtained free of charge from The Cambridge Crystallographic Data Centre via www.ccdc.cam.ac.uk/data_request/cif (or from the Cambridge Crystallographic Data Centre, 12 Union Road, Cambridge CB21EZ, UK; fax: (+44)1223-336-033; or deposit@ccdc.cam.ac.uk).

Gas Sorption. Nitrogen isotherms were measured using a TRIFLEX apparatus (Micromeritics) at −196 °C. The sample was transferred from a sealed ampoule to the sample holder inside a glove box. Before the analysis, 50 mg of the thoroughly washed **MUV-3** were degassed at 150 °C and $\sim 5\times10^{-6}$ bar overnight. The BET surface area was calculated by using the Brunauer−Emmett−Teller equation, and micropore volume was calculated by the t-plot method.

The high-pressure CO_2 adsorption isotherms were measured in a gravimetric sorption analyzer IGA-100 (Hiden Isochema). 50 mg of adsorbent were placed in a sample holder and before measurement, the sample was degassed 3 hours at 100 °C under vacuum. CO_2 adsorption isotherms were acquired at 10, 25, 35 and 55 °C.

The NO adsorption isotherms were collected in a Micromeritics ASAP 2010 apparatus. In the first experiment, 200 mg of fresh **MUV-3** were placed in the sample holder and activated at 100 ºC under vacuum overnight. Then, the isotherm was measured at 0 ºC up to 1 bar. In order to distinguish between physisorption and chemisoption, a second isotherm was measured on the same sample but degassing at room temperature, assuming that only the physisorbed molecules were removed.

Infrared spectra. IR were recorded in a Platinum-ATR diamond Bruker spectrometer in the 4000−350 cm^{-1} range using powdered samples.

Synthesis of **NC-MUV-3.** The controlled thermal treatment of **MUV-3** is carried out in a CVD oven at low temperature of 700 ºC under nitrogen atmosphere (ramp rate of 2 ºC·min^{-1}) keeping the material at that temperature for 3.5 h. This process yields a black powdered carbon material, which is subsequently treated in 0.5 M H_2SO_4 solution for 6 h in order to remove residual metals. The resulting sample is thoroughly washed with ethanol and dried at 80 ºC, obtaining a nanocomposite (NC) denoted as NC-MUV-3. This reaction was carried out three times with similar electrocatalyst values for the three different batches. Details on the structural characterization of the NC can be found in the Supporting Information (section S5).

Electrochemical characterization of NC-MUV-3. The electrochemical experiments were performed using an Autolab electrochemical workstation (PGSTAT-128N potentiostat/galvanostat) connected to a personal computer that uses Nova 2.1 electrochemical software. The powdered materials were mixed with acetylene black and PVDF in a mass ratio of 80:10:10 in ethanol and deposited on a nickel foam or carbon felt electrode. The as-prepared electrodes were dried overnight at 80 ºC and pressed. Each working electrode contained about 0.20–0.30 mg·cm^{-2} of electroactive material and had a geometric surface area of about 0.2 cm^2. A typical three-electrode experimental cell equipped with a stainless-steel plate having 4 cm^2 of surface area as the counter electrode, and a Metrohm Ag/AgCl (3 M KCl) as the reference electrode was used for the electrochemical characterization of the working electrodes. All measurements were carried out with magnetic agitation and nitrogen bubbling. In addition, chronoamperometric studies were performed at a constant overpotential (j = 0.3 and 0.4 V), and chronopotentiometric studies at constant current densities of 10 and 15 mA·cm^{-2}. All potentials reported in this manuscript were converted to the RHE reference scale using E(RHE) = E(NHE) + 0.059·pH = Eº(Ag/AgCl) + 0.197 V + 0.059·pH; and to the OP reference scale using OP = E(NHE)-0.4 V, where E(NHE) = E(Ag/AgCl) + 0.197V.

ASSOCIATED CONTENT

Supporting Information

AUTHOR INFORMATION

Corresponding Author

*guillermo.minguez@uv.es

Author Contributions

‡These authors contributed equally.

Notes

The authors declare no competing financial interests.

ACKNOWLEDGMENT

The work has been supported by the European Union (ERC-2016-CoG 724681-S-CAGE and ERC-2018-StG 804110-2D-PnictoChem) and the Spanish MINECO (Structures of Excellence María de Maeztu MDM-2015-0538 and Severo Ochoa SEV-2016-0683; projects CTQ2014-59209-P,

CTQ2017-89528-P and MAT2015-71842-P). G.M.E. and M.G.-M. thank MICINN for a "Ramón y Cajal" and a "Juan de la Cierva – Incorporación" fellowships, respectively. J.L.-C. acknowledges the Universitat de València for an "Atracció de Talent" grant. G.A. thanks support by the Generalitat Valenciana (CIDEGENT/2018/001), and the Deutsche Forschungsgemeinschaft (DFG; FLAG-ERA AB694/2-1). Dr. F. Hauke and Prof. A. Hirsch are acknowledged for their kind support with the Raman equipment.

REFERENCES

(1) Maurin, G.; Serre, C.; Cooper, A.; Férey, G. The new age of MOFs and of their porous-related solids. *Chem. Soc. Rev.* **2017**, *46*, 3104–3107.

(2) Wang, L. J.; Deng, H.; Furukawa, H.; Gándara, F.; Cordova, K. E.; Peri, D.; Yaghi, O. M. Synthesis and characterization of metal–organic framework-74 containing 2, 4, 6, 8, and 10 different metals. *Inorg. Chem.* **2014**, *53*, 5881–5883.

(3) Caskey, S. R.; Wong-Foy, A. G.; Matzger, A. J. Dramatic tuning of carbon dioxide uptake via metal substitution in a coordination polymer with cylindrical pores. *J. Am. Chem. Soc.* **2008**, *130*, 10870–10871.

(4) (a) Bloch, E. D.; Queen, W. L.; Krishna, R.; Zadrozny, J. M.; Brown, C. M.; Long, J. R. Hydrocarbon separations in a metal-organic framework with open iron(II) coordination sites. *Science.* **2012**, *335*, 1606–1610. (b). Queen, W. L.; Hudson, M. R.; Bloch, E. D.; Mason, J. A.; Gonzalez, M. I.; Lee, J. S.; Gygi, D.; Howe, J. D.; Lee, K.; Darwish, T. A.; James, M.; Peterson, V. K.; Teat, S. J.; Smit, B.; Neaton, J. B.; Long, J. R.; Brown, C. M. Comprehensive study of carbon dioxide adsorption in the metal–organic frameworks M_2(dobdc) (M = Mg, Mn, Fe, Co, Ni, Cu, Zn). *Chem. Sci.* **2014**, *5*, 4569–4581.

(5) Park, K. S.; Ni, Z.; Côté, A. P.; Choi, J. Y.; Huang, R.; Uribe-Romo, F. J.; Chae, H. K.; O'Keeffe, M.; Yaghi, O. M. Exceptional chemical and thermal stability of zeolitic imidazolate frameworks. *Proc. Natl. Acad. Sci. U. S. A.* **2006**, *103*, 10186–10191.

(6) Huang, X.-C.; Lin, Y.-Y.; Zhang, J.-P.; Chen, X.-M. Ligand-directed strategy for zeolite-yype metal–organic frameworks: zinc(II) imidazolates with unusual zeolitic topologies. *Angew. Chem. Int. Ed.* **2006**, *45*, 1557–1559.

(7) Banerjee, R.; Phan, A.; Wang, B.; Knobler, C.; Furukawa, H.; O'Keeffe, M.; Yaghi, O. M. High-throughput synthesis of zeolitic imidazolate frameworks and application to CO_2 capture. *Science.* **2008**, *319*, 939–943.

(8) Tian, Y.-Q.; Yao, S.-Y.; Gu, D.; Cui, K.-H.; Guo, D.-W.; Zhang, G.; Chen, Z.-X.; Zhao, D.-Y. Cadmium imidazolate frameworks with polymorphism, high thermal stability, and a large surface area. *Chem. Eur. J.* **2010**, *16*, 1137–1141.

(9) Horike, S.; Kadota, K.; Itakura, T.; Inukai, M.; Kitagawa, S. Synthesis of magnesium ZIF-8 from $Mg(BH_4)_2$. *Dalton Trans.* **2015**, *44*, 15107–15110.

(10) Kadota, K.; Sivaniah, E.; Bureekaew, S.; Kitagawa, S.; Horike, S. Synthesis of manganese ZIF-8 from $[Mn(BH_4)_2 \cdot 3THF] \cdot NaBH_4$. *Inorg. Chem.* **2017**, *56*, 8744–8747.

(11) (a) Brozek, C. K.; Miller, J. T.; Stoian, S. A.; Dinca, M. NO Disproportionation at a mononuclear site-isolated Fe^{2+} center in Fe^{2+}-MOF-5. *J. Am. Chem. Soc.* **2015**, *137*, 7495–7501. (b) Liu, X.; Zhou,

Y.; Zhang, J.; Tang, L.; Luo, L.; Zeng, G. Iron containing metal–organic frameworks: structure, synthesis, and applications in environmental remediation. *ACS Appl. Mater. Interfaces* **2017**, *9*, 20255–20275. (c) Osadchii, D. Y.; Olivos-Suarez, A. I.; Szécsényi, Á.; Li, G.; Nasalevich, M. A.; Dugulan, I. A.; Crespo, P. S.; Hensen, E. J. M.; Veber, S. L.; Fedin, M. V.; Sankar, G.; Pidko, E. A.; Gascon, J. Isolated Fe sites in metal organic frameworks catalyze the direct conversion of methane to methanol. *ACS Catal.* **2018**, *8*, 5542–5548.

(12) McKinlay, A. C.; Eubank, J. F.; Wuttke, S.; Xiao, B.; Wheatley, P. S.; Bazin, P.; Lavalley, J.-C.; Daturi, M.; Vimont, A.; De Weireld, G.; Horcajada, P.; Serre, C.; Morris, R. E. Nitric oxide adsorption and delivery in flexible MIL-88(Fe) metal–organic frameworks. *Chem. Mater.* **2013**, *25*, 1592–1599. (b) Bloch, E. D.; Queen, W. L.; Chavan, S.; Wheatley, P. S.; Zadrozny, J. M.; Morris, R.; Brown, C. M.; Lamberti, C.; Bordiga, S.; Long, J. R. Gradual release of strongly bound nitric oxide from $Fe_2(NO)_2$(dobdc). *J. Am. Chem. Soc.* **2015**, *137*, 3466–3469. (c) Brozek, C. K.; Miller, J. T.; Stoian, S. A.; Dincă, M. NO disproportionation at a mononuclear site-isolated Fe^{2+} center in Fe^{2+}-MOF-5. *J. Am. Chem. Soc.* **2015**, *137*, 7495–7501.

(13) Phan, A.; Doonan, C. J.; Uribe-Romo, F. J.; Knobler, C. B.; O'Keeffe, M.; Yaghi, O. M. Synthesis, structure, and carbon dioxide capture properties of zeolitic imidazolate frameworks. *Acc. Chem. Res.* **2010**, *43*, 58–67.

(14) (a) Liu, B.; Shioyama, H.; Akita, T.; Xu, Q. Metal-organic framework as a template for porous carbon synthesis. *J. Am. Chem. Soc.* **2008**, *130*, 5390–5391. (b) Santos, V. P.; Wezendonk, T. A.; Jaén, J. J. D.; Dugulan, A. I.; Nasalevich, M. A.; Islam, H.-U.; Chojecki, A.; Sartipi, S.; Sun, X.; Hakeem, A. A.; Koeken, A. C. J.; Ruitenbeek, M.; Davidian, T.; Meima, G. R.; Sankar, G.; Kapteijn, F.; Makkee, M.; Gascon, J. Metal organic framework-mediated synthesis of highly active and stable Fischer-Tropsch catalysts. *Nat. Commun.* **2015**, *6*, 6451. (c) Cao, X.; Tan, C.; Sindoro, M.; Zhang, H. Hybrid micro-/nano-structures derived from metal–organic frameworks: preparation and applications in energy storage and conversion. *Chem. Soc. Rev.* **2017**, *46*, 2660–2677; (d) Dang, S.; Zhu, Q.-L.; Xu, Q. Nanomaterials derived from metal–organic frameworks. *Nat. Rev. Mater.* **2017**, *3*, 17075; Zhang, H.; Liu, X.; Wu, Y.; Guan, C.; Cheetham, A.K.; Wang, J. MOF-derived nanohybrids for electrocatalysis and energy storage: current status and perspectives. *Chem. Commun*. **2018**, *54*, 5268.

(15) Zhao, D.; Shui, J. L.; Grabstanowicz, L. R.; Chen, C.; Commet, S. M.; Xu, T.; Lu, J.; Liu, D. J. Highly efficient non-precious metal electrocatalysts prepared from one-pot synthesized zeolitic imidazolate frameworks. *Adv. Mater.* **2014**, *26*, 1093–1097.

(16) (a) Zhao, D.; Shui, J.-L.; Chen, C.; Chen, X.; Reprogle, B. M.; Wang, D.; Liu, D.-J. Iron imidazolate framework as precursor for electrocatalysts in polymer electrolyte membrane fuel cells. *Chem. Sci.* **2012**, *3*, 3200. (b) Zheng, R.; Liao, S.; Hou, S.; Qiao, X.; Wang, G.; Liu, L.; Shu, T.; Du, L. A hollow spherical doped carbon catalyst derived from zeolitic imidazolate framework nanocrystals impregnated/covered with iron phthalocyanines. *J. Mater. Chem. A* **2016**, *4*, 7859–7868. (c) Chen, Y.; Ji, S.; Wang, Y.; Dong, J.; Chen, W.; Li, Z.; Shen, R.; Zheng, L.; Zhuang, Z.; Wang, D.; Li, Y. Isolated single iron atoms anchored on N-doped porous carbon as an efficient electrocatalyst for the Oxygen Reduction Reaction. *Angew. Chem. Int. Ed.* **2017**, *56*, 6937–6941.

(17) (a) Seel, F.; Wende, P.; Marcolin, H. E.; Trautwein, A. T.; Maeda, Y. Iron(II) compounds of imidazoles. *Zeitschrift für Anorg. und Allg. Chemie* **1976**, *426*, 198–204. (b) Spek, A. L.; Duisenberg, A. J. M.; Feiters, M. C. The structure of the three-dimensional polymer poly[μ-

hexakis(2-methylimidazolato-N,N′)-triiron(II)], $[Fe_3(C_4H_5N_2)_6]_n$. *Acta Crystallogr. Sect. C Cryst. Struct. Commun.* **1983**, *39*, 1212–1214. (c) Rettig, S. J.; Storr, A.; Summers, D. A.; Thompson, R. C.; Trotter, J. Transition metal azolates from metallocenes. 2. Synthesis, X-ray structure, and magnetic properties of a three-dimensional polymetallic iron(ii) imidazolate complex, a low-temperature weak ferromagnet. *J. Am. Chem. Soc.* **1997**, *119*, 8675–8680. (d) Rettig, S. J.; Storr, A.; Summers, D. A.; Thompson, R. C.; Trotter, J. Iron(II) 2-methylimidazolate and copper(ii) 1,2,4-triazolate complexes: systems exhibiting long-range ferromagnetic ordering at low temperatures. *Can. J. Chem*. **1999**, *77*, 425–433 (e) López-Cabrelles, J.; Mañas-Valero, S.; Vitórica-Yrezábal, I. J.; Bereciartua, P. J.; Rodríguez-Velamazán, J. A.; Waerenborgh, J. C.; Vieira, B. J. C.; Davidovikj, D.; Steeneken, P. G.; van der Zant, H. S. J.; Mínguez Espallargas, G.; Coronado, E. Isoreticular two-dimensional magnetic coordination polymers prepared through pre-synthetic ligand functionalization. *Nat. Chem.* **2018**, *10*, 1001–1007.

(18) Beldon, P. J.; Fábián, L.; Stein, R. S.; Thirumurugan, A.; Cheetham, A. K.; Friščić, T. Rapid room-temperature synthesis of zeolitic imidazolate frameworks by using mechanochemistry. *Angew. Chem. Int. Ed.* **2010**, *49*, 9640–9643.

(19) Huang, X.; Zhang, J.; Chen, X. $[Zn(Bim)_2]\cdot(H_2O)_{1.67}$: A metal-organic open-framework with sodalite topology. *Chinese Sci. Bull.* **2003**, *48*, 1531.

(20) Avci, C.; Ariñez-Soriano, J.; Carné-Sánchez, A.; Guillerm, V.; Carbonell, C.; Imaz, I.; Maspoch, D. Post-synthetic anisotropic wet-chemical etching of colloidal sodalite ZIF crystals. *Angew. Chem. Int. Ed.* **2015**, *54*, 14417–14421.

(21) Fairen-Jimenez, D.; Moggach, S. A.; Wharmby, M. T.; Wright, P. A.; Parsons, S.; Düren, T. Opening the gate: framework flexibility in ZIF-8 explored by experiments and simulations. *J. Am. Chem. Soc.* **2011**, *133*, 8900–8902

(22) McKinlay, A. C.; Xiao, B.; Wragg, D. S.; Wheatley, P. S.; Megson, I. L.; Morris, R. E. Exceptional behavior over the whole adsorption−storage−delivery cycle for NO in porous metal organic frameworks. *J. Am. Chem. Soc.* **2008**, *130*, 10440–10444.

(23) Xiao, B.; Wheatley, P. S.; Zhao, X.; Fletcher, A. J.; Fox, S.; Rossi, A. G.; Megson, I. L.; Bordiga, S.; Regli, L.; Thomas, K. M.; Morris, R. E. High-capacity hydrogen and nitric oxide adsorption and storage in a metal−organic framework. *J. Am. Chem. Soc.* **2007**, *129*, 1203–1209.

(24) Hinks, N. J.; McKinlay, A. C.; Xiao, B.; Wheatley, P. S.; Morris, R. E. Metal organic frameworks as NO delivery materials for biological applications. *Micropor. Mesopor. Mater.* **2010**, 129, 330–334.

(25) Mai, H. D.; Rafiq, K.; Yoo, H. Nano metal-organic framework-derived inorganic hybrid nanomaterials: synthetic strategies and applications. *Chem. Eur. J.* **2017**, *23*, 5631–5651. (b) Kaneti, Y. V.; Tang, J.; Salunkhe, R. R.; Jiang, X.; Yu, A.; Wu, K. C. W.; Yamauchi, Y. Nanoarchitectured design of porous materials and nanocomposites from metal-organic frameworks. *Adv. Mater.* **2017**, *29*, 1604898. (c) Xia, W.; Mahmood, A.; Zou, R.; Xu, Q. Metal–organic frameworks and their derived nanostructures for electrochemical energy storage and conversion. *Energy Environ. Sci.* **2015**, *8*, 1837–1866. (d) Liu, J.; Zhu, D.; Guo, C.; Vasileff, A.; Qiao, S. Z. Design strategies toward advanced MOF-derived electrocatalysts for energy-conversion reactions. *Adv. Energy Mater.* **2017**, *7*, 1700518. (e) Liang, Z.; Qu, C.; Guo, W.; Zou, R.; Xu, Q. Pristine metal-organic frameworks and their composites for energy storage and conversion. *Adv. Mater.* **2018**, *30*, 1702891. (f) Guan, B. Y.; Yu, X. Y.; Wu, H. Bin; Lou, X. W. D. Complex

nanostructures from materials based on metal–organic frameworks for electrochemical energy storage and conversion. *Adv. Mater.* **2017**, *29*, 1703614. (g) Shen, K.; Chen, X.; Chen, J.; Li, Y. Development of MOF-derived carbon-based nanomaterials for efficient catalysis. *ACS Catal.* **2016**, *6*, 5887–5903. (h) Sun, J.-K.; Xu, Q. Functional materials derived from open framework templates/precursors: synthesis and applications. *Ener. Environ. Sci.* **2014**, *7*, 2071–2100. (i) Wu, H. Bin; Lou, X. W. Metal-organic frameworks and their derived materials for electrochemical energy storage and conversion: promises and challenges. *Sci. Adv.* **2017**, *3*, eaap9252. (j) Qian, Y.; Khan, I. A.; Zhao, D. Electrocatalysts derived from metal-organic frameworks for oxygen reduction and evolution reactions in aqueous media. *Small* **2017**, *13*, 1701143. (k) Wang, W.; Xu, X.; Zhou, W.; Shao, Z. Recent progress in metal-organic frameworks for applications in electrocatalytic and photocatalytic water splitting. *Adv. Sci.* **2017**, *4*, 1600371. (l) Wang, H.; Zhu, Q.-L.; Zou, R.; Xu, Q. Metal-organic frameworks for energy applications. *Chem* **2017**, *2*, 52–80. (m) Barkholtz, H. M.; Liu, D.-J. Advancements in rationally designed PGM-free fuel cell catalysts derived from metal–organic frameworks. *Mater. Horizons* **2017**, *4*, 20–37.

(26) Chaikittisilp, W.; Hu, M.; Wang, H.; Huang, H.-S.; Fujita, T.; Wu, K. C.-W.; Chen, L.-C.; Yamauchi, Y.; Ariga, K. Nanoporous carbons through direct carbonization of a zeolitic imidazolate framework for supercapacitor electrodes. *Chem. Commun.* **2012**, *48*, 7259.

(27) Xia, B. Y.; Yan, Y.; Li, N.; Wu, H. Bin; Lou, X. W.; Wang, X. A Metal–organic framework-derived bifunctional oxygen electrocatalyst. *Nat. Ener.* **2016**, *1*, 15006.

(28) Gadipelli, S.; Zhao, T.; Shevlin, S. A.; Guo, Z. Switching effective oxygen reduction and evolution performance by controlled graphitization of a cobalt–nitrogen–carbon framework system. *Energy Environ. Sci.* **2016**, *9*, 1661–1667.

(29) Wang, Z.; Lu, Y.; Yan, Y.; Larissa, T. Y. P.; Zhang, X.; Wuu, D.; Zhang, H.; Yang, Y.; Wang, X. Core-shell carbon materials derived from metal-organic frameworks as an efficient oxygen bifunctional electrocatalyst. *Nano Energy* **2016**, *30*, 368–378.

(30) Zhao, J.; Quan, X.; Chen, S.; Liu, Y.; Yu, H. Cobalt nanoparticles encapsulated in porous carbons derived from core-shell ZIF67@ZIF8 as efficient electrocatalysts for Oxygen Evolution Reaction. *ACS Appl. Mater. Interfaces* **2017**, *9*, 28685–28694.

(31) Romero, J.; Rodriguez-San-Miguel, D.; Ribera, A.; Mas-Ballesté, R.; Otero, T. F.; Manet, I.; Licio, F.; Abellán, G.; Zamora, F.; Coronado, E. Metal-functionalized covalent organic frameworks as precursors of supercapacitive porous N-doped graphene. *J. Mater. Chem. A* **2017**, *5*, 4343–4351.

(32) Dou, S.; Li, X.; Tao, L.; Huo, J.; Wang, S. Cobalt nanoparticle-embedded carbon nanotube/porous carbon hybrid derived from MOF-encapsulated Co_3O_4 for oxygen electrocatalysis. *Chem. Commun.* **2016**, *52*, 9727–9730.

(33) Dionigi, F.; Strasser, P. NiFe-based (oxy)hydroxide catalysts for Oxygen Evolution Reaction in non-acidic electrolytes. *Adv. Energy Mater.* **2016**, *6*, 1600621.

(34) Lu, X.; Zhao, C. Electrodeposition of hierarchically structured three-dimensional nickel–iron electrodes for efficient oxygen evolution at high current densities. *Nat. Commun.* **2015**, *6*, 6616.

(35) Stassen, I.; Styles, M.; Grenci, G.; Van Gorp, H.; Vanderlinden, W.; De Feyter, S.; Falcaro, P.; De Vos, D.; Vereecken, P.; Ameloot, R. Chemical vapour deposition of zeolitic imidazolate framework thin films. *Nat. Mater.* **2016**, *15*, 304–310.

(36) (a) Sheldrick, G. M. Crystal structure refinement with SHELXL. *Acta Crystallogr. Sect. C Struct. Chem.* **2015**, *71*, 3–8. (b) Dolomanov, O. V., Bourhis, L. J., Gildea, R. J., Howard, J. A. K. & Puschmann, H. OLEX2: a complete structure solution, refinement and analysis program. *J. Appl. Crystallogr.* **2009**, *42*, 339–341.